On the Effect of Stabilization Methods for Quaternion Invariants on the Uncertainty in Optimization-based Estimation ⋆

Fabian Girrbach [*,**] **Jeroen D. Hol** [*] **Raymond Zandbergen** [*]
Robin Verschueren [**] **Giovanni Bellusci** [*] **Moritz Diehl** [**]

[*] *Xsens Technologies B.V., 7521 PR Enschede, the Netherlands (e-mail: firstname.lastname@xsens.com).*
[**] *Department of Microsystems Engineering (IMTEK), University of Freiburg, 79110 Freiburg, Germany (e-mail: firstname.lastname@imtek.uni-freiburg.de)*

Abstract: The handling of 3D orientations is a common element in many problems that arise in the estimation and control of dynamic systems. Over-parametrizations such as unit quaternions are commonly used to avoid singularities but come with the property of an invariant which needs to be preserved. By using numerical optimization methods, these invariants are subject to numeric errors and require stabilization. In this work, we adopt methods known from optimal control for the problem of state estimation. We present an optimization-based attitude estimator using the measurements of an inertial measurement unit and evaluate the performance of a first-order stabilization of the invariant by modifying the dynamics. The uncertainties of the estimator are analyzed for different configurations of the proposed stabilization. Finally, we show how the stabilization affects the estimation of parameters and justify the use of an additional equality constraint for the invariant to yield more robust and consistent results.

Keywords: Estimation algorithms, optimal estimation, invariants, attitude algorithms.

1. INTRODUCTION

In the age of the internet of moving things, the ability to track motion becomes a feature of major importance. Driven by recent developments in sensor technology, a rising number of applications in robotics, augmented and virtual reality is equipped with motion sensors such as *inertial measurement unit*s (IMUs). The acquired measurement data from multiple sensors is fused to estimate the motion state of the dynamic system using estimation algorithms. The most famous approach addressing the problem of state estimation in real-time is the Kalman (1960) filter, as well as its extensions for nonlinear systems, *extended Kalman filter* (EKF) and *unscented Kalman filter* (UKF) (Julier and Uhlmann, 1997). An increase in system complexity and the coherently increasing demands on performance and robustness of systems such as *unmanned aerial vehicle*s (UAVs), push traditional methods for control and estimation towards their limits. Supported by recent advances in embedded computing technology and efficient numerical algorithms, optimization-based methods aim to manage the balancing act between performance and real-time requirements.

The motion state may consider typical quantities such as position, velocity, and more importantly the attitude or orientation of the object of interest w.r.t. a fixed reference frame. The latter is represented in the SO(3) rotation group which describes all rotations about the origin in the 3-dimensional Euclidean space. Due to its straightforward interpretation, Euler angles are probably the most commonly used representation of the attitude. However, Euler angles suffer from a difficulty which is often referred to as gimbal lock and results in the loss of a degree of freedom in specific configurations. Another disadvantage of Euler angles is that they result in a strongly nonlinear system of equations when expressing the dynamics of a system.
Higher order representations (see Shuster (1993) for an overview) are used in practice to avoid this pitfall but need to be restricted in their degrees of freedom. Unit quaternions are one valid representation with significant practical relevance. Quaternions are an extension of complex numbers to four dimensions, where the quaternion is defined by

$$\boldsymbol{q} = [q_0, q_1, q_2, q_3]^\intercal = [q, \breve{\boldsymbol{q}}^\intercal]^\intercal \tag{1}$$

consisting of a scalar $q \in \mathbb{R}$ and vector part $\breve{\boldsymbol{q}} \in \mathbb{R}^3$. For the valid representation of rotations in SO(3) the quaternion needs to be restricted to a valid manifold by defining $\boldsymbol{q} \in \mathcal{Q} := \{\boldsymbol{q} \in \mathbb{R}^4 \mid \|\boldsymbol{q}\|^2 = 1\}$ to be of unit norm. The property needs to be preserved to ensure a valid interpretation of the attitude leaving 3 degrees of freedom. Using numerical methods with limited precision introduces errors which can cause a violation of this condition over time and result in undefined behavior.

⋆ This work is supported by the project AWESCO (H2020-ITN-642682) funded by the European Union's Horizon 2020 research and innovation program under the Marie Sklodowska-Curie grant agreement No. 642682. Jeroen D. Hol contributed to this work during his former employment at Xsens Technologies B.V..

In this paper, we use a first order stabilization of the quaternion invariant by modifying the system dynamics. After establishing the necessary notation and operators in Section 2, we explain the problems arising from the violation of the unit norm constraint and present possible methods to stabilize the numerics in Section 3. The methods are applied to a simple attitude estimation problem using measurement data of a *magnetic, angular rate & gravity* (MARG) sensor in Section 4. The results of the *moving horizon estimation* (MHE)-based estimator are compared in Section 5.

2. QUATERNION NOTATION

The concatenation of orientations is defined by the quaternion multiplication, for which we adopt the $\odot$ operator

$$\boldsymbol{q} \odot \boldsymbol{p} = [q_0 p_0 - \breve{\boldsymbol{q}}^\intercal \breve{\boldsymbol{p}}, (q_0 \breve{\boldsymbol{p}} + \breve{\boldsymbol{q}} \times \breve{\boldsymbol{p}})^\intercal]^\intercal, \tag{2}$$

for $\boldsymbol{q}, \boldsymbol{p} \in \mathcal{Q}$.

For arbitrary coordinate systems A and B with relative orientation $\boldsymbol{q}_{AB}$, the vector ${}_B\boldsymbol{r} \in \mathbb{R}^3$ in coordinate frame B can be expressed in the coordinate frame A using

$$\begin{bmatrix} 0 \\ {}_A\boldsymbol{r} \end{bmatrix} = \boldsymbol{q}_{AB} \odot \begin{bmatrix} 0 \\ {}_B\boldsymbol{r} \end{bmatrix} \odot \boldsymbol{q}_{AB}^{-1} \tag{3}$$

$${}_A\boldsymbol{r} = (2q_{AB}^2 - 1)\,{}_B\boldsymbol{r} + 2q_{AB}\,{}_B\boldsymbol{r}\breve{\boldsymbol{q}}_{AB}^\times + 2\breve{\boldsymbol{q}}_{AB}(\breve{\boldsymbol{q}}_{AB}^\intercal\,{}_B\boldsymbol{r}),$$

where $\breve{\boldsymbol{q}}_{AB}^\times$ denotes the skew-symmetric matrix

$$\breve{\boldsymbol{q}}_{AB}^\times = \begin{bmatrix} 0 & -q_1 & q_2 \\ q_3 & 0 & -q_3 \\ -q_2 & q_1 & 0 \end{bmatrix} \tag{4}$$

of the vector part $\breve{\boldsymbol{q}}_{AB}$ of the orientation quaternion $\boldsymbol{q}_{AB}$. Using this result, we define a function

$$R(\boldsymbol{q}_{AB}) = (2q_{AB}^2 - 1)I_3 + 2q_{AB}\breve{\boldsymbol{q}}_{AB}^\times + 2\breve{\boldsymbol{q}}_{AB}\breve{\boldsymbol{q}}_{AB}^\intercal, \tag{5}$$

to obtain an orthonormal rotation matrix $R \in \mathbb{R}^{3\times3}$ which is used in the following equations to simplify the mathematical notation.

3. STABILIZATION METHODS

Violations of the unit norm of an orientation quaternion can result rapidly in undefined behavior of a system. Several methods exist to restrict the quaternions to a valid manifold in $SO(3)$. In this work, we use modified system dynamics and impose equality constraints to ensure a valid manifold. A different approach is to use an exponential mapping and use its Lie algebra (see Bloesch et al. (2016) for an introduction).

3.1 Invariant Stabilization using Dynamics

A commonly used method to preserve invariants against numerical drift is to modify the dynamics by extending the *ordinary differential equation* (ODE) of the state variable with a weighted penalization term. For second order invariants this method is known as Baumgarte stabilization (Baumgarte, 1972) and for an orientation state represented as a unit quaternion, the following first order stabilization

$$\dot{\boldsymbol{q}}_{AB} = \underbrace{\frac{1}{2}\boldsymbol{q}_{AB} \odot [0, {}_B\boldsymbol{\omega}^\intercal]^\intercal}_{\dot{\boldsymbol{q}}_{\text{natural}}} + \underbrace{\frac{\rho}{2}\boldsymbol{q}_{AB}((\boldsymbol{q}_{AB}^\intercal\boldsymbol{q}_{AB})^{-1} - 1)}_{\dot{\boldsymbol{q}}_{\text{corr}}} \tag{6}$$

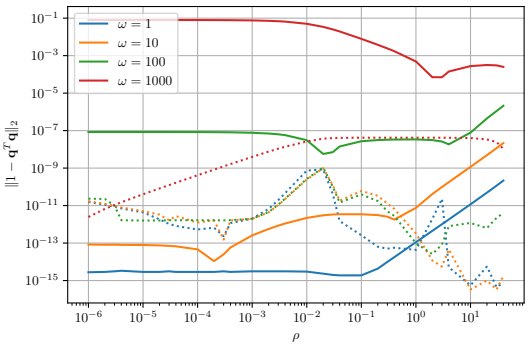

Fig. 1. Invariant violation as a function of the stabilization contraction term ρ after integration of a constant angular velocity signal $\boldsymbol{\omega}$ over $T_f = 100$ s using a fixed step size of $\Delta t = 0.01$ s. The *solid* lines are obtained using an explicit RK4 integrator whereas the *dotted* lines show the results for an implicit RK integrator using $s = 3$ Lagrange polynomials $l(\tau)$ at Legendre collocation points.

is explained in detail by Gros et al. (2015) and widely used in the aerospace community (Martin and Salan, 2010). The correction term, denoted as $\dot{\boldsymbol{q}}_{\text{corr}}$, was shown to be orthogonal to the natural ODE of a unit quaternion $\dot{\boldsymbol{q}}_{\text{natural}}$. The additional term $\dot{\boldsymbol{q}}_{\text{corr}}$ increases the stiffness of the equation which can cause numerical problems when using explicit integration methods. To solve stiff equations, we use an *implicit Runge-Kutta* (IRK) method of the form

$$\boldsymbol{x}_{k+1} = \boldsymbol{x}_k + \Delta t \sum_{j=1}^{s} \kappa_j \int_0^1 l_j(\tau)\mathrm{d}\tau, \qquad k = 1, \dots N, \tag{7}$$

where $s \in \mathbb{N}$ orthogonal Lagrange polynomials $l(\tau)$ are integrated over $\tau \in \mathbb{R}$ using the corresponding coefficients $\kappa \in \mathbb{R}$. The integration result is scaled using the step size Δt to propagate the state $\boldsymbol{x}_k$. The contraction factor in $\dot{\boldsymbol{q}}_{\text{corr}}$ is denoted by $\rho \in \mathbb{R}$ and needs to be chosen carefully. Fig. 1 shows the invariant violation of the unit quaternion $\boldsymbol{q}_{AB}$ after an integration time $T_f = 100$ s as a function of ρ for a few different constant angular velocity inputs using explicit and implicit *Runge-Kutta* (RK) integrators with a fixed step size of $\Delta t = 0.01$ s. The plot visualizes that the explicit methods are more sensitive to the choice of the contraction parameter ρ than implicit integrators which reveal a more equally good performance for different angular velocity signals $\boldsymbol{\omega}$.

3.2 Invariant Stabilization using Equality Constraints

Another approach to preserve the unit norm property of the quaternion is to impose the condition as a further equality constraint into the optimization problem. Using direct methods (Betts, 2010) constraints of the form

$$(\boldsymbol{q}_{AB}^{[k]})^\intercal \boldsymbol{q}_{AB}^{[k]} - 1 = 0, \qquad k = 1, \dots N \tag{8}$$

can be imposed at discrete times t_k in the estimation window $T = N\Delta t$. One could think, that imposing the unit norm at each discrete time t_k could improve the preservation of the unit norm condition but the use of several invariant constraints might over-constrain the problem and could lead to convergence issues and undesired results.

4. MHE ATTITUDE ESTIMATOR USING MARG SENSOR

In this section, we introduce a standard example for an attitude estimator using a 9-axis motion sensor including a 3-axis accelerometer, a 3-axis gyroscope, and magnetometer, correctly referred to as MARG sensor but often called IMU. The device measures the local magnetic field, angular rate, linear acceleration and is typically rigidly attached to a moving object.

4.1 Models

Following the model description similar to Sabatini (2006) and Skoglund et al. (2017), we design a optimization-based attitude estimator using MHE. The state vector $\boldsymbol{x}(t) \in \mathbb{R}^{n_x}$ is defined by

$$\boldsymbol{x} = [\boldsymbol{q}_{LS}^\intercal, {}^a_S\boldsymbol{\delta}^\intercal, {}^m_S\boldsymbol{\delta}^\intercal]^\intercal, \tag{9}$$

where we dropped the evaluation point t for notational convenience. $\boldsymbol{q}_{LS} \in \mathcal{Q}$ encodes the relative orientation between the sensor frame S and the local-fixed frame L as a unit quaternion. The states ${}^a_S\boldsymbol{\delta}, {}^m_S\boldsymbol{\delta} \in \mathbb{R}^3$ correspond to the bias terms for accelerometer and magnetometer in the sensor frame S. The vector $\boldsymbol{u} \in \mathbb{R}^{n_u}$ contains the angular rate measurements of the gyroscope

$$\boldsymbol{u} = [{}_S\boldsymbol{\omega}_{LS}], \tag{10}$$

where ${}_S\boldsymbol{\omega}_{LS} \in \mathbb{R}^3$. The predicted measurements of accelerometer and magnetometer can be calculated using the sensor models

$$ {}^a h(\boldsymbol{x}) = R(\boldsymbol{q}_{SL})\, {}_L\boldsymbol{g} + {}^a_S\boldsymbol{\delta}, \tag{11a}$$

$$ {}^m h(\boldsymbol{x}) = R(\boldsymbol{q}_{SL})\, {}_L\boldsymbol{e} + {}^m_S\boldsymbol{\delta}, \tag{11b}$$

where ${}_L\boldsymbol{g} \in \mathbb{R}^3$ and ${}_L\boldsymbol{e} \in \mathbb{R}^3$ denote the gravity and earth magnetic field vector in the local frame L. In this example, these vectors are assumed to be constant. In a magnetic-distorted environment a calibration procedure (Kok et al., 2012) is required to achieve similar behavior. Furthermore, we made use of the following identity

$$R(\boldsymbol{q}_{SL}) = R(\boldsymbol{q}_{LS}^{-1}) \tag{12}$$

for the definition of the sensor models.

The bias terms are assumed to be constant over the estimation window, whereas the propagation of the orientation is defined by the ODE,

$$\begin{aligned}\dot{\boldsymbol{q}}_{LS} &= \frac{1}{2}\boldsymbol{q}_{LS} \odot [0, {}_S\boldsymbol{\omega}_{LS}^\intercal]^\intercal \\ &= \frac{1}{2}\begin{bmatrix} 0 & -{}_S\boldsymbol{\omega}_{LS}^\intercal \\ {}_S\boldsymbol{\omega}_{LS} & {}_S\boldsymbol{\omega}_{LS}^\times \end{bmatrix}\boldsymbol{q}_{LS} \end{aligned} \tag{13a}$$

$$ {}^a_S\dot{\boldsymbol{\delta}} = [0,0,0]^\intercal, \tag{13b}$$

$$ {}^m_S\dot{\boldsymbol{\delta}} = [0,0,0]^\intercal. \tag{13c}$$

4.2 Optimization Problem

To solve the attitude estimation problem using nonlinear optimization methods over a time horizon T, we encode the estimation problem in a continuous-time objective function

$$f(\boldsymbol{x}(\cdot)) = \frac{1}{2}\int_{\tau=t-T}^{t} \Big[\| {}_S\boldsymbol{a}(t) - {}^a h(\boldsymbol{x}(\tau)) \|^2_{{}^aR^{-1}} \tag{14a}$$

$$ + \| {}_S\boldsymbol{m}(t) - {}^m h(\boldsymbol{x}(\tau)) \|^2_{{}^mR^{-1}} \Big]\, d\tau \tag{14b}$$

$$ + \frac{1}{2}\|\boldsymbol{x}(t-T) - \hat{\boldsymbol{x}}(t-T)\|^2_{P^{-1}}. \tag{14c}$$

The squared residuals of accelerometer ${}_S\boldsymbol{a} \in \mathbb{R}^3$ and magnetometer ${}_S\boldsymbol{m} \in \mathbb{R}^3$ measurements and their corresponding sensor models are normalized according to their standard deviations using weighting matrices ${}^aR = I_3\, {}^a\sigma^2$ and ${}^mR = I_3\, {}^m\sigma^2$ accordingly. To account for previous measurements or a priori information a further cost term is introduced in (14c). This cost term, often referred to as arrival cost, penalizes deviations of the first state estimate in the current horizon $\boldsymbol{x}(t-T)$ from an a priori known and therefore as constant entering term $\hat{\boldsymbol{x}}(t-T)$ according to the weighting matrix P. The objective function does not include a term for the process noise on the tracked horizon. Therefore the angular rate does not enter as optimization variable in the problem.

We use a direct multiple shooting approach (Bock and Plitt, 1984), which is well understood for optimal control problems and allows the handling of nonlinearities by lifting the problem and leads to a discretization of states $(\boldsymbol{x}_0, \dots, \boldsymbol{x}_N)$ and inputs $(\boldsymbol{u}_0, \dots, \boldsymbol{u}_{N-1})$ where the estimation horizon $T = N\Delta t$ is defined by a multiple $N \in \mathbb{N}$ of the sampling time $\Delta t \in \mathbb{R}$. Applying the discretization to (14) leads to the following equality constrained optimization problem:

$$\min_{\boldsymbol{x}_0,\cdots,\boldsymbol{x}_N} \quad \frac{1}{2}\sum_{k=0}^{N} \left\| \begin{bmatrix} {}_S\boldsymbol{a}_k \\ {}_S\boldsymbol{m}_k \end{bmatrix} - \begin{bmatrix} {}^a h(\boldsymbol{x}_k) \\ {}^m h(\boldsymbol{x}_k) \end{bmatrix} \right\|^2_{R_k^{-1}} + \frac{1}{2}\|\boldsymbol{x}_0 - \hat{\boldsymbol{x}}_0\|^2_{P^{-1}} \tag{15a}$$

$$\text{s.t.} \quad \boldsymbol{x}_{k+1} = \phi(\boldsymbol{x}_k, \boldsymbol{u}_k), \quad k = 0, \dots, N-1 \tag{15b}$$

$$ Z_{\boldsymbol{q}}(\boldsymbol{x}_N)^\intercal Z_{\boldsymbol{q}}(\boldsymbol{x}_N) = 1, \tag{15c}$$

where R weighting matrix denotes the block-diagonal concatenation of the measurement noises ${}^aR$ and ${}^mR$

$$R_k = \begin{bmatrix} {}^aR_k & 0 \\ 0 & {}^mR_k \end{bmatrix}, \quad k = 0, \dots, N \tag{16}$$

The shooting constraints are imposed using the IRK integrator function $\phi(\boldsymbol{x}_k, \boldsymbol{u}_k)$ which propagates the state using the ODEs defined Eq. (13). An additional and optional constraint (15c) enforces the unit norm property of the quaternion using a selection matrix $Z_{\boldsymbol{q}}$ for the quaternion entries in $\boldsymbol{x}$ at the end of the horizon.

4.3 Arrival Cost Computation

The arrival cost incorporates a priori knowledge about the state to keep the computational cost manageable concerning real-time constraints of a system. Whereas Michalska and Mayne (1995) proposed to use a constant arrival cost term others Haseltine and Rawlings (2005); Ferreau et al. (2012) use a penalization term on the initial guess $\hat{\boldsymbol{x}}_0$ which is weighted according to the inverse of the covariance matrix denoted as P. To update $\hat{\boldsymbol{x}}_0^{[i]}$ and $P^{[i]}$ before shifting the horizon by Δt to $[i+1]$, we apply the smoothed EKF arrival cost update which is summarized for quaternion estimation in the following algorithm:

(1) Get result from the optimizer $\boldsymbol{x}_0^{*[i]}$ and constant entering parameters $\hat{\boldsymbol{x}}_0^{[i]}$,$P^{[i]}$,$R^{[i]}$ for each run i after shifting the tracked horizon of the MHE estimator.

(2) Compute Kalman gain $K^{[i]}$ using the Jacobian of the measurement model:

$$H^{[i]} = \begin{bmatrix} \nabla_{\boldsymbol{x}}\, {}^{a}h(\boldsymbol{x}) \\ \nabla_{\boldsymbol{x}}\, {}^{m}h(\boldsymbol{x}) \end{bmatrix}\Bigg|_{\boldsymbol{x}_0^{*[i]}} \tag{17a}$$

$$K^{[i]} = P^{[i]} H^{[i]\intercal}((H^{[i]} P^{[i]} H^{[i]\intercal}) + R_0^{[i]})^{-1} \tag{17b}$$

(3) Calculate new initial guess for arrival cost $\hat{\boldsymbol{x}}_{0,i+1}$:

$$\boldsymbol{x}_0^{[i+1]} = \boldsymbol{x}_0^{[i]} + K^{[i]} \left(\begin{bmatrix} {}_S\boldsymbol{a}_0^{[i]} \\ {}_S\boldsymbol{m}_0^{[i]} \end{bmatrix} - \begin{bmatrix} {}^{a}h(\boldsymbol{x}_0^{*[i]}) \\ {}^{m}h(\boldsymbol{x}_0^{*[i]}) \end{bmatrix} - H^{[i]}(\hat{\boldsymbol{x}}_0^{[i]} - \boldsymbol{x}_0^{*[i]}) \right) \tag{18a}$$

$$\hat{\boldsymbol{x}}_0^{[i+1]} = \phi(\boldsymbol{x}_0^{[i]}, \boldsymbol{u}_1^{[i]}) \tag{18b}$$

(4) Update arrival cost covariance matrix using the calculated Kalman gain $K^{[i]}$:

$$\tilde{P}^{[i]} = (I_{N_x} - K^{[i]} H^{[i]}) P^{[i]} \tag{19}$$

(5) Calculate the process noise matrix $Q_0^{[i]}$ using the bias instability of accelerometer ${}^{\delta_a}\Sigma \in \mathbb{R}^{3\times3}$, magnetometer ${}^{\delta_m}\Sigma \in \mathbb{R}^{3\times3}$ and the measurement noise of the gyroscope which is expressed as a quaternion using

$${}^{q}\Sigma(\boldsymbol{q}) = \frac{\Delta t}{2} \begin{bmatrix} \breve{\boldsymbol{q}}^{\times} + q_0 I_3 \\ \breve{\boldsymbol{q}}^{\intercal} \end{bmatrix} {}^{\omega}\Sigma \begin{bmatrix} \breve{\boldsymbol{q}}^{\times} + q_0 I_3 \\ \breve{\boldsymbol{q}}^{\intercal} \end{bmatrix}^{\intercal} \tag{20a}$$

$$Q^{[i]} = \begin{bmatrix} {}^{q}\Sigma(\boldsymbol{q}_{LS,0}^{[i]}) & 0 & 0 \\ 0 & {}^{\delta_a}\Sigma & 0 \\ 0 & 0 & {}^{\delta_m}\Sigma \end{bmatrix} \tag{20b}$$

(6) Propagate covariance matrix using the Jacobian of the dynamics:

$$\Phi^{[i]} = \nabla_{\boldsymbol{x}} \phi(\boldsymbol{x}, \boldsymbol{u})|_{\boldsymbol{x}_0^{*[i]}} \tag{21a}$$

$$P^{[i+1]} = \Phi^{[i]} \tilde{P}^{[i]} \Phi^{[i]\intercal} + Q^{[i]} \tag{21b}$$

We want to stress that the measurement noise of the gyroscope enters over the process noise matrix Q only in the computation of the arrival cost and is not considered in the optimization problem. This represents a strong assumption which does not allow the use of very large horizons.

4.4 State Uncertainty Computation

In the previous section, we described the smoothed EKF update for the covariance matrix P which is used for the weighted quadratic arrival cost term containing the prior knowledge of the past. To calculate the state uncertainty of the estimator at the current time $t_{N,i}$, we invert the *Karush-Kuhn-Tucker* (KKT) system of the current optimization problem. The KKT system is defined as the block-concatenation of the Hessian of the Lagrangian $\mathcal{L}(\boldsymbol{x}, \lambda)$ and the gradient of the equality constraints $g(\boldsymbol{x})$ yielding the matrix

$$\begin{bmatrix} \nabla^2_{\boldsymbol{x}} \mathcal{L}(\boldsymbol{x}, \lambda) & \nabla_{\boldsymbol{x}} g(\boldsymbol{x}) \\ \nabla_{\boldsymbol{x}} g(\boldsymbol{x})^{\intercal} & 0 \end{bmatrix}. \tag{22}$$

For a real-time critical implementation of such an estimator a fast Schur complement method (see Bürger et al. (2017)) might be the preferred solution to compute the covariance of the state rather than inverting the whole KKT matrix.

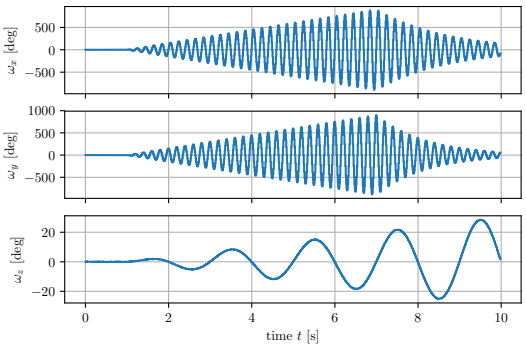

Fig. 2. Simulated angular velocity signal ${}_S\boldsymbol{\omega} = [\omega_x, \omega_y, \omega_z]^{\intercal}$ using high frequent sine and cosine signals with changing amplitude for ω_x and ω_y and a low frequent increasing sine signal for the ω_z-channel. The continuous signals are sampled with a frequency of 100 Hz over a total simulation time of 10 s.

5. NUMERICAL EXAMPLE

5.1 Simulation

To analyze the proposed methods in Section 3 and their influence on the estimation result, we simulate a control input signal and assume the initial orientation to be $\boldsymbol{q}_{LS} = [1, 0, 0, 0]^{\intercal}$. A series of in amplitude changing sine and cosine signals is used to excite the system. The resulting angular velocity signal is shown in Fig. 2. To obtain more general results, we use several independent runs with additional Gaussian noise with 0-mean and a standard deviation of ${}^{\omega}\sigma$. By applying the measurement models defined in (11) to the simulated state trajectory and adding the corresponding biases and measurement noises, we obtain the simulated measurements. The measurements of the accelerometer are expressed in its natural physical unit, whereas the magnetometer measurements are expressed in pseudo-units representing the magnetic field vector of unit length. The necessary mapping to such a unit can be achieved after a calibration procedure. All simulation parameters are summarized in Table 1.

Table 1. Simulation Parameters

Variable	Symbol	Value	Unit
Sim. time	T	10	s
Sampling time	Δt	0.01	s
Initial orientation	$\boldsymbol{q}_{LS_0}$	$[0, 0, 0]^{\intercal}$	deg
Gyroscope stddev	${}^{\omega}\sigma$	$4.5 \cdot 10^{-4}$	degs^{-1}
Accelerometer stddev	${}^{a}\sigma$	0.0186	ms^{-2}
Accelerometer bias	${}^{a}\delta$	0.11	ms^{-2}
Magnetometer stddev	${}^{m}\sigma$	0.08	
Magnetometer bias	${}^{m}\delta$	0.15	

5.2 Results

The simulated control input and measurements of an IMU are used in this Section to estimate the attitude using the moving horizon estimator explained in Section 4. The estimator needs to be initialized with an initial guess for the state values and covariances. All initial conditions for the estimator are summarized in Table 2.

Table 2. Initial Conditions for Estimator

Variable	Symbol	Value	Unit
Orientation	$\boldsymbol{q}_{LS_0}$	$[10, -15, 5]^\intercal$	deg
Accelerometer bias	${}^{a}_{S}\boldsymbol{\delta}$	$[0, 0, 0]^\intercal$	ms^{-2}
Magnetometer bias	${}^{m}_{S}\boldsymbol{\delta}$	$[0, 0, 0]^\intercal$	
Orientation stddev	$\sigma_{q_{LS}}$	0.15	
Accelerometer stddev	${}^{a}\sigma$	0.02	ms^{-2}
Magnetometer stddev	${}^{m}\sigma$	0.1	

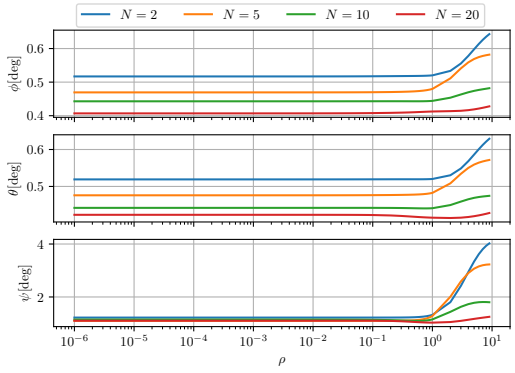

Fig. 3. RMSEs as a function of the first order stabilization contraction parameter ρ for different horizon lengths N.

The estimator was implemented using the symbolic optimization framework CasADi (Andersson et al., 2018) and solved using the interior point solver IPOPT (Wächter and Biegler, 2005). The framework allows us to run the estimator for a set of different horizon lengths $N = \{2, 5, 10, 20\}$. A comparison of the estimated orientation and the simulated ground truth data for different values parameters of the contraction factor ρ is shown in Fig. 3. The calculated *root mean square error* (RMSE) reveals that the estimation performance does not primarily depend on the contraction factor ρ. For all values of $\rho \leq 1$ the RMSEs show only small deviations which are invisible for the plotted range. Furthermore, the estimation performance improves for larger horizons N and therefore a horizon length $N = 20$ results in the lowest RMSE.

Even though the evaluation of the mean values of the estimated states does not reveal significant differences for different contraction factors ρ, it may be too early to judge about its importance. Analyzing the standard deviations calculated from the inverse of the KKT matrix at the current solution of the optimizer $\boldsymbol{x}^{*[i]}$ reveals some interesting behavior of the estimated uncertainty of the accelerometer bias. Fig. 5a shows the estimated standard deviations of the bias for each channel for a horizon length of $N = 5$. For the x and y-channel, we see the expected result for all different values of ρ. Due to the initial orientation and the lack of excitation during the first second of simulation, the bias in x and y-direction is not observable and does not change a lot compared to its initial value. The same arguments lead to the conclusion that the bias in z-direction should be well observable due to the signal of the gravity vector. Fig. 5a shows that this expected behavior is only achieved for values of $\rho \geq 0.1$. The reason for this behavior can be explained with the help of Fig. 4, which shows the standard deviations extracted

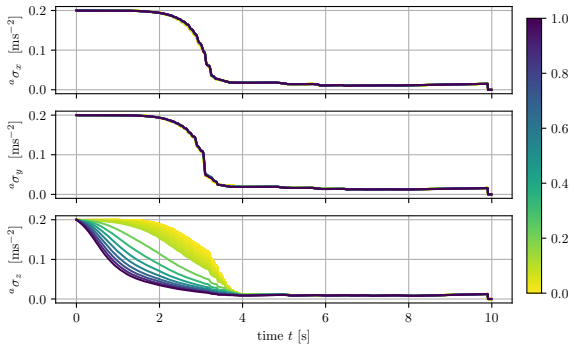

Fig. 4. Estimated standard deviations of the arrival cost covariance matrix P for the accelerometer bias. Each line shows the result for a specific value of the contraction parameter ρ and is colored according to the color bar.

from the covariance matrix $P^{[i]}$ during the calculation of smoothed EKF arrival cost update. A larger contraction parameter ρ has a tightening effect on the arrival cost. Deviations from, as prior knowledge in the optimization problem entering, $\hat{\boldsymbol{x}}_0^{[i]}$ will therefore be penalized stronger for larger values of ρ. The tightening effect is introduced over the Jacobian matrix $\Phi^{[i]}$ of the dynamic model $\phi(\boldsymbol{x}, \boldsymbol{u})$ as described in Section 4.3. It is important to note that the explained phenomena is not primarily driven by a big change in the orientation uncertainty. The estimated standard deviations of roll, pitch and yaw are not affected by an increasing contraction parameter ρ. The online identification of parameters, such as biases, is crucial in the field of state estimation. Therefore, the variations of the estimated standard deviations, as seen in Fig. 5a, are undesired and may lead under different conditions to a bad estimation performance. By using an additional equality constraint (15c) at the end of the estimation window, the estimated standard deviations show increased robustness to changes of the contraction parameter ρ. Fig. 5b reveals the expected standard deviation result for the accelerometer bias. The bias in z-direction becomes directly observable in the first second of simulation and increases slightly as soon as the system gets excited. The biases in x and y-direction stay at their initial value until they become observable due to the excitation of the system and converge asymptotically to a constant value defined by the respective noise terms.

6. CONCLUSION

The use of over-parametrizations, such as quaternions for orientation states successfully avoids phenomena such as the gimbal lock and is therefore recommended for estimation tasks in three dimensional space. These higher order representations impose invariants to restrict its degree of freedom. To guarantee that the invariants are satisfied, the present study used a first-order stabilization of the dynamics. Using a simple example of an MHE-based attitude estimator, we showed how the contraction factor in the stabilization term can influence the estimation of the standard deviations of the arrival cost and the current state estimate. The contraction parameter ρ has a tighten-

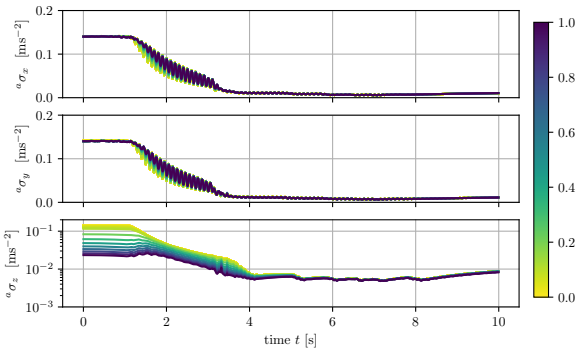

(a)

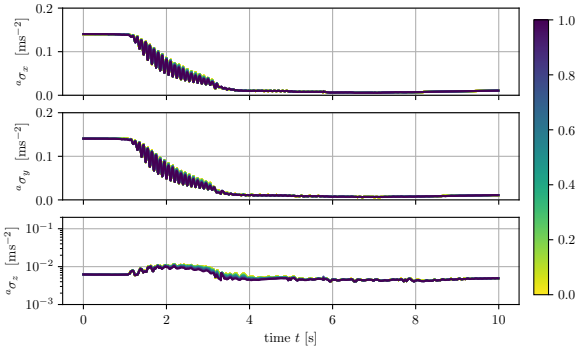

(b)

Fig. 5. Estimated standard deviation σ of the accelerometer bias for each channel x, y, z over simulation time t with (b) and without (a) using an additional equality constraint at the end of each estimation window. Each line shows the result for a specific value of the contraction parameter ρ and is colored according to the color bar.

ing effect on the arrival cost when calculated using the EKF smoothed arrival cost update. As a result, the past has a stronger impact on the current estimate. Even though this is an interesting feature to increase the robustness of the estimator, it should not influence the estimated standard deviations under well-performing conditions. To generalize the estimated standard deviations, we introduced the use of an additional equality constraint at the end of estimation horizon. The proposed method yields the expected standard deviations and is robust to changes of the contraction parameter of the stabilization.

REFERENCES

Andersson, J.A.E., Gillis, J., Horn, G., Rawlings, J.B., and Diehl, M. (2018). CasADi – A software framework for nonlinear optimization and optimal control. *Mathematical Programming Computation*.

Baumgarte, J. (1972). Stabilization of constraints and integrals of motion in dynamical systems. *Computer Methods in Applied Mechanics and Engineering*, 1(1), 1–16. doi:10.1016/0045-7825(72)90018-7.

Betts, J.T. (2010). *Practical Methods for Optimal Control and Estimation Using Nonlinear Programming*. Society for Industrial and Applied Mathematics. doi:10.1137/1.9780898718577.

Bloesch, M., Sommer, H., Laidlow, T., Burri, M., Nuetzi, G., Fankhauser, P., Bellicoso, D., Gehring, C., Leutenegger, S., Hutter, M., and Siegwart, R. (2016). A primer on the differential calculus of 3d orientations. *arXiv.org*.

Bock, H. and Plitt, K. (1984). A multiple shooting algorithm for direct solution of optimal control problems. *IFAC Proceedings Volumes*, 17(2), 1603–1608. doi:10.1016/s1474-6670(17)61205-9.

Bürger, A., Kouzoupis, D., Altmann-Dieses, A., and Diehl, M. (2017). A schur complement method for optimum experimental design in the presence of process noise. *IFAC-PapersOnLine*, 50(1), 14118–14124. doi:10.1016/j.ifacol.2017.08.1853.

Ferreau, H.J., Kraus, T., Vukov, M., Saeys, W., and Diehl, M. (2012). High-speed moving horizon estimation based on automatic code generation. In *2012 IEEE 51st IEEE Conference on Decision and Control (CDC)*. IEEE. doi:10.1109/cdc.2012.6426428.

Gros, S., Zanon, M., and Diehl, M. (2015). Baumgarte stabilisation over the SO(3) rotation group for control. In *2015 54th IEEE Conference on Decision and Control (CDC)*. IEEE. doi:10.1109/cdc.2015.7402298.

Haseltine, E.L. and Rawlings, J.B. (2005). Critical evaluation of extended kalman filtering and moving-horizon estimation. *Industrial & Engineering Chemistry Research*, 44(8), 2451–2460. doi:10.1021/ie034308l.

Julier, S.J. and Uhlmann, J.K. (1997). New extension of the kalman filter to nonlinear systems. In I. Kadar (ed.), *Signal Processing, Sensor Fusion, and Target Recognition VI*. SPIE. doi:10.1117/12.280797.

Kalman, R.E. (1960). A new approach to linear filtering and prediction problems. *Transactions of the ASME–Journal of Basic Engineering*, 82(Series D), 35–45. doi:10.1115/1.3662552.

Kok, M., Hol, J.D., Schn, T.B., Gustafsson, F., and Luinge, H. (2012). Calibration of a magnetometer in combination with inertial sensors. In *Proc. 15th Int. Conf. Information Fusion*, 787–793.

Martin, P. and Salan, E. (2010). Design and implementation of a low-cost observer-based attitude and heading reference system. *Control Engineering Practice*, 18(7), 712–722. doi:10.1016/j.conengprac.2010.01.012.

Michalska, H. and Mayne, D. (1995). Moving horizon observers and observer-based control. *IEEE Transactions on Automatic Control*, 40(6), 995–1006. doi:10.1109/9.388677.

Sabatini, A. (2006). Quaternion-based extended kalman filter for determining orientation by inertial and magnetic sensing. *IEEE Transactions on Biomedical Engineering*, 53(7), 1346–1356. doi:10.1109/tbme.2006.875664.

Shuster, M.D. (1993). Survey of attitude representations. *Journal of the Astronautical Sciences*, 41, 439–517.

Skoglund, M.A., Sjanic, Z., and Kok, M. (2017). On orientation estimation using iterative methods in euclidean space. In *2017 20th International Conference on Information Fusion (Fusion)*. IEEE. doi:10.23919/icif.2017.8009830.

Wächter, A. and Biegler, L.T. (2005). On the implementation of an interior-point filter line-search algorithm for large-scale nonlinear programming. *Mathematical Programming*, 106(1), 25–57. doi:10.1007/s10107-004-0559-y.